# Kinetics of Lipid Rearrangements during Poly(ethylene glycol)-Mediated Fusion of Highly Curved Unilamellar Vesicles†

Kervin O. Evans and Barry R. Lentz*

*Department of Biochemistry and Program in Molecular & Cellular Biophysics, University of North Carolina, Chapel Hill, North Carolina 27599-7260*

*Received July 19, 2001; Revised Manuscript Received October 23, 2001*

ABSTRACT: In an effort to increase our understanding of the molecular rearrangements that occur during lipid bilayer fusion, we have used different fluorescent probes to characterize the lipid rearrangements associated with poly(ethylene glycol) (PEG)-mediated fusion of DOPC:$DL_{18:3}$PC (85:15) small, unilamellar vesicles (SUVs). Unlike in our previous studies of fusion kinetics [Lee, J., and Lentz, B. R., *Biochemistry 36,* 6251−6259], these vesicles have mean diameters of 20 nm compared to 45 nm. Surprisingly, we found significant inter-vesicle lipid mixing at 5 wt % PEG, well below the PEG concentration required (17.5 wt %) for vesicles fusion. Lipid movement rate between bilayers (or inter-leaflet movement) increased abruptly at 10 wt % PEG, and the rate of lipid mixing increased thereafter with increasing amounts of PEG. The characteristic time of lipid mixing between outer leaflets ($\tau \approx 24$ s) was comparable to that observed at and above PEG concentrations needed to induce fusion (17.5 wt %) of either 20 or 45 nm vesicles. We also found that slower lipid mixing ($\tau \approx 267$ s) between fusing vesicles occurred on the same time scale or slightly faster than vesicle contents mixing ($\tau \approx 351$ s). In addition, our measurements showed that lipids redistributed across the bilayer on a time scale just slightly faster than pore formation ($\tau \approx 217$ s). This is the first demonstration of trans-bilayer movement of lipids during fusion. We also found that water was excluded from the bilayer ($\tau \approx 475$ s) during product maturation. These observations suggest that fusion in smaller vesicles (∼20 nm) proceeds via a multistep mechanism similar to that we reported for somewhat larger vesicles, except that two intermediates are no longer clearly resolved.

Advances made in cellular research over the past few years have defined many aspects of the membrane fusion events involved in such biological processes as viral infection (*1*−*3*), exocytosis (*4*−*6*), and endocytosis (*7*). In the cell, proteins are required both to regulate and drive the fusion process (*8*, *9*). However, because of the complexity of the required lipid rearrangements and of the protein machines that drive them, little is known about the mechanism by which this occurs. In efforts to understand the detailed lipid rearrangements during fusion, our lab has studied the fusion process in simple membrane vesicles composed of synthetic lipids and induced to fuse by the aggregating polymer poly(ethylene) glycol (PEG) (*10*). Using PEG, close inter-bilayer approach can be accomplished in the absence of proteins (*11*). We have previously established the parallel between PEG-mediated vesicle fusion and biomembrane fusion (*12*). Thus, the first step of the fusion process entailed transient proton movement between vesicles and transient capacitance changes in influenza virus hemagglutinin (HA)-expressing cells and secretory granule (SG) cells. At the same time, contacting membrane leaflets exchanged lipids during PEG-mediated fusion on a time scale and with an activation energy comparable to that seen in HA-mediated fusion. Second, there was a delay of comparable duration to that seen for HA-mediated and SG fusion between the initial transient pore/lipid mixing and fusion pore formation. Finally, the rate and activation energy of fusion pore formation was comparable in PEG-mediated fusion to that seen in HA-mediated fusion. This parallelism means that we can use the relatively simple PEG-mediated fusion process to learn about the process that protein machines must mediate in cells.

Despite all we know about PEG-mediated fusion, many questions remain about fusion in simple vesicle systems. For instance, we know that lipids move in a directed fashion from the outer leaflet to the inner leaflet of fusing vesicles by the end of fusion (*13*). But, when do the lipids actually move across the bilayer during fusion? We know further that there is significant lipid mixing between the outer leaflets of aggregated vesicles just prior to the mixing of inner leaflets and contents (*14*) in fusing (at 17.5 wt % PEG) 45 nm vesicles. At what rate does lipid mixing proceed under subfusion PEG concentrations (<17.5 wt % PEG)? In addition, is the two-intermediate process of vesicular fusion preserved for vesicles of limited smaller diameters (20 nm)? Finally, it has been well documented that packing stresses are considerably different in smaller vesicles versus larger ones (*15*, *16*). We know that this packing strain must be relieved upon completion of fusion because vesicles increase in diameter during fusion (*17*). But, when are these stresses relieved during fusion? In this paper, we attempt to further our understanding of fusion in DOPC:$DL_{18:3}$PC[1] sonicated vesicles by answering these questions. We found that PEG-

† Supported by USPHS Grant GM 32707 to B.R.L.

* To whom correspondence should be addressed. Phone: (919) 966-5384. Fax: (919) 966-2852. E-mail: uncbrl@med.unc.edu.

10.1021/bi011508x CCC: $22.00 
Published on Web 12/29/2001

mediated fusion followed the same basic three-step model as proposed for 45 nm vesicles (*14*), but there was no longer the clear delay between the initial and final steps of fusion as seen for 45 nm vesicles.

## EXPERIMENTAL PROCEDURES

### *Materials*

Chloroform stock solutions of 1,2-dioleoyl-3-*sn*-phospatidylcholine (DOPC), *N*-(7-nitro-2,1,3-benzoxadiazol-4-yl)-1,2-dioleoyl-3-*sn*-phospatidylserine (NBD-PS), and powdered stock samples of 1,2-dilinolenyl-*sn*-phosphatidylcholine ($DL_{18:3}PC$) were purchased from Avanti Polar Lipids, Inc. (Alabaster, AL). Powdered forms of 2-(4,4-difluoro-5-methyl-4-bora-3a,4a-diaza-*s*-indacene-3-dodecanoyl)-1-hexadecanoyl-*sn*-glycero-3-phosphocholine ($\beta$-BODIPY 500/510 $C_{12}$−HPC or BODIPY-500-PC) and 2-(4,4-difluoro-5,7-diphenyl-4-bora-3a,4a-diaza-*s*-indacene-3-dodecanoyl)-1-hexadecanoyl-*sn*-glycero-3-phosphoethanolamine ($\beta$-BODIPY 530/550 $C_{12}$−HPE or BODIPY-530-PE) were purchased from Molecular Probes (Eugene, OR). These lipids were used without further purification, and the concentrations were determined by phosphate assay (*18*). Dipicolinic acid (DPA) and *N*-tris[hydroxymethyl]methyl-2-aminoethanesulfonic acid (TES) were purchased from Sigma Chemical Company (St. Louis, MO). $TbCl_3$ was purchased from Johnson Matthey Catalog Company (Ward Hill, MA). Sodium dithionite was purchased from Fluka BioChemika (Ronkonkoma, NY). Ethylenediamine tetraacetic acid (EDTA) and carbowax poly(ethylene glycol) (PEG, molecular weight 7000−9000) 8000 were purchased from Fisher Scientific (Fair Lawn, NJ). PEG was purified as described earlier (*19*). Octaethyleneglycol mono-*n*-dodecyl ether ($C_{12}E_8$) was purchased from CalBiochem (La Jolla, CA). All other materials were of ACS reagent grade or the highest purity available.

### *Methods*

*Vesicle Preparation.* Small, unilamellar vesicles (SUVs) were prepared as previously described by Lentz et al. (*20*) from freeze-dried mixtures of DOPC and $DL_{18:3}PC$ (85:15 molar ratio) that had been mixed in $CHCl_3$ prior to freeze-drying. Sonicated vesicle samples were fractionated by centrifugation for 25 min using a Beckman TL-100 ultracentrifuge (Palo Alto, CA) at 70 000 rpm and 4 °C. Large, unilamellar vesicles (LUVs) were prepared by extruding multilamellar vesicles 7 times through a 0.1 $\mu$m polycarbonate filter under a pressure of about 75 psi of argon to generate LUVs approximately 100 nm in diameter (*21*).

*Determination of Vesicle Size.* Vesicle diameters were measured by quasi-elastic light scattering (QELS) using a custom-built multiangle instrument (*19*) that incorporates a computing autocorrelator from Particle Sizing Systems, Inc. (Santa Barbara, CA). Data collection and analysis were controlled by software purchased from Particle Sizing System. Vesicle size was calculated using a solid-particle model in the volume-weighted mode. Details of the procedure are reported elsewhere (*11*). All experiments were done at 23 °C unless otherwise stated. All vesicles were approximately 20 nm in mean diameter with a Gaussian half width of approximately 3.8 nm. However, upon diluting vesicles incubated in 17.5 wt % PEG for 10 min to <1 wt % PEG, the mean size of the fusion product was 48 nm, which would imply fusion product resulting from fusion within an aggregate having 6−8 SUVs.

*Bodipy Membrane Mixing Assays.* We used the photostable probe pair of $\beta$-BODIPY500−HPC/530-HPE to monitor total lipid mixing as recently described by Malinin et al. (*22*). Briefly, lipid samples of DOPC:$DL_{18:3}PC$ (85:15) were dried under argon with both BODIPY probes incorporated at 0.5 mol % and lyophilized overnight. Vesicles were prepared from both probe-free and probe-containing lipid samples as above (buffer was 1 mM EDTA, 2 mM TES, 100 mM NaCl, pH 7.4). The change in fluorescence due to dilution of the probe pair into probe-free vesicles was monitored on an SLM/Aminco-48000 spectrofluorometer (SLM-Aminco Instruments, Rochester, NY) operating in T-format and equipped with a focused 450 W xenon lamp. The excitation monochromator was set at 500 nm (slits at 4 × 4). Emission for Bodipy500 was monitored at 520 nm (slits at 8 × 8) in channel A, and an OG-550 cutoff filter (Schott Glass Technologies, Duryea, PA) was used for Bodipy530 in channel B. Prior to measurements, probe-containing and probe-free vesicles were mixed at 1:4 (0.5 mM final total SUV concentration). An appropriate amount of PEG was then added to obtain the desired concentration. The ratio of donor (Bodipy500 in channel A) to acceptor (Bodipy530 in channel B) fluorescence was converted to lipid mixing fraction (LM) as described elsewhere (*22*).

*Inner Leaflet Mixing Assay.* Inner leaflet mixing was monitored as in Lee and Lentz (*14*). Briefly, NBD-PS was incorporated at 10:1 lipid-to-probe ratio in SUVs, and the outer leaflet probes were reduced with dithionite at 200:1 dithionite-to-probe ratio (*14*, *23*, *24*) so that only the inner leaflet probes exhibited a fluorescence lifetime. Vesicles were then passed down a Sephadex G-75 column to remove the dithionite. Probe vesicles were mixed with probe-free vesicles at 1:5 ratio in a buffer containing 1 mM EDTA, 2 mM TES, and 100 mM NaCl prior to adding the appropriate amount of PEG. Lifetime measurements were made on an SLM-Aminco 48000 spectrofluorometer as previously described (*14*). A beam spreader was used to minimize any photolysis of the probe. An increase in the average fluorescence lifetime indicated that NBD-PS in the inner leaflet was diluted during fusion. The fraction of inner leaflet mixing (ILM) was calculated as previously described (*25*).

*$Tb^{+3}$/DPA Contents Mixing and Leakage Assay.* Mixing of trapped aqueous contents was monitored using the $Tb^{3+}$/DPA assay (*26*) as previously adapted for use in the presence of PEG (*27*, *28*). The buffer was modified from previous reports as follows: (1) the contents mixing buffers contained 8 mM $TbCl_2$, 10 mM TES, 60 mM NaCl, and 10 mM TES, 80 mM DPA; (2) the column buffer contained 1 mM $CaCl_2$, 1 mM EDTA, 2 mM TES, 100 mM NaCl. Any unencapsu-

[1] Abbreviations: DOPC, 1,2-dioleoyl-*sn*-phospatidlycholine; NBD-PS, *N*-(7-nitro-2,1,3-benzoxdiazol-4-yl)-1,2-dioleoyl-3-*sn*-phosphatidylserine; $DL_{18:3}PC$, 1,2-dilinoleoyl-*sn*-phosphatidylcholine; BODIPY500, 2-(4,4-difluoro-5-methyl-4-bora-3a,4a-diaz-*s*-indacene-3-dodecanoyl)-1-hexadecanoyl-*sn*-glycero-3-phosphocholine; BODIPY530, 2-(4,4-difluoro-5-methyl-4-bora-3a,4a-diaz-*s*-indacene-3-dodecanoyl)-1-hexadecanoyl-*sn*-glycero-3-phosphoethanolamine; DPA, dipicolinic acid; $Tb^{3+}$, terbium ion; EDTA, ethylenediaminetetraacetic acid; $C_{12}E_8$, octaethyleneglycol mono-*n*-dodecyl ether; SUVs, small unilamellar vesicles; TES, *N*-[tris(hydroxymethyl)-methyl]-2-aminoethane sulfonic acid; LUVs, large unilamellar vesicles; Det, detergent; LM, lipid mixing; ILM, inner leaflet mixing; CM, contents mixing; TBM, transbilayer movement.

lated $Tb^{3+}$ and DPA were removed by passing the vesicle samples down a Sephadex G75 column equilibrated with the column buffer. For contents mixing, vesicles were premixed at a 1:1 ratio ($Tb^{3+}$:DPA) and added to the appropriate PEG solution for monitoring contents mixing. The final vesicle concentration was 0.5 mM. Contents mixing fraction (CM) and leakage were calculated as described previously (*27*).

*Transbilayer Lipid Movement Assay.* NBD-PS is a fluorescently labeled lipid that has a very low rate of random flip across the bilayer (*13*). Because of this low rate of lipid flip-flop, we used it to monitor directed trans-bilayer movement of lipids during fusion. NBD-PS was incorporated (100:1 lipid-to-probe ratio) in lipid samples prepared as above and sonicated to form SUVs. Vesicles (0.5 mM) and PEG were mixed in an amber vial at 23 °C and periodically vortexed. Aliquots of 75 $\mu$L were removed from the mixed stock of SUVs at indicated times and quickly dumped into buffer at 4 °C (*29*) to dilute the PEG 20-fold, arrest fusion, and slow any further lipid movement. The total fluorescence ($F_{tot}$) of the sample was measured, and dithionite (20 $\mu$L of 5 M stock) was added to reduce all outer-leaflet probes. Since dithionite does not permeate the bilayer (*13*, *24*), the remaining fluorescence should be from only those probes located in the inner leaflet ($F_{in}$). After a fully stable fluorescence signal was recorded, $C_{12}E_8$ was added to obtain background fluorescence ($F_o$) by exposing all probes to dithionite. The fraction of total probe that was found in the inner leaflet was calculated as $R = F_{in} - F_o/F_{tot} - F_o$. Excitation was at 460 nm (4 × 4 slits), and emission was at 524 nm (16 × 16 slits). An OG-515 cutoff filter was used in the emission light path to reduce scattered light. This assay was done in the presence of 17.5 and 20 wt % PEG as interleaflet lipid movement does not occur in these vesicles below these concentrations (*13*).

*Changes in Lipid Packing during Fusion.* Fluorophores with exchangeable protons can undergo deuterium exchange that causes an increase in quantum yield because of reduced nonradiative decay via excited-state proton transfer (*30*). Thus, for TMA-DPH, the ratio of its lifetime in $D_2O$ to that in $H_2O$ depends on the degree of water exposure to the exchangeable protons (*31*, *32*). The exchangeable protons affected are located in the headgroup region of TMA-DPH (*33*) that is thought to be located in the membrane interface region (*34*). Therefore, this lifetime ratio should reflect hydration of the bilayer interface region (*32*).

A small aliquot (0.04−0.08 vol % of vesicle sample) of stock TMA-DPH in methanol (0.8 mM) was added to SUVs in 1 mM EDTA, 2 mM TES, and 100 mM NaCl (pH 7.4) buffer at 0.5 mM to achieve a lipid:probe ratio of 250:1. Vesicles were incubated for 10 min with vigorous mixing prior to measurements. Phase shifts and modulation ratios of TMA-DPH fluorescence were collected on an SLM-Aminco spectrofluorometer. The excitation was in the region of 351.1 to 363.8 nm of a Coherent Inova-90 argon-ion laser UV multiline, with a 3 mm KV-450 filter (Schott Optic Glass, Duryea, PA) used in the emission path to reduce scattered light. A beam spreader was used to defocus the laser and minimize photolysis. Phase shift and modulation ratios were collected and converted to average lifetime as described elsewhere (*17*).

*Curve-Fitting and Statistical Treatment of Data.* All data were fitted to curves (solid lines) using Sigma Plot 6.0 (SPSS, Inc.). The curve-fitting was based on nonlinear least-squares estimation of the parameters using the Marquardt−Levenberg algorithm as implemented by Sigma Plot. Parameter uncertainties are standard errors of the parameter estimate returned by this procedure. The abilities of a single exponential and then a double exponential model to describe time courses were tested. In every case, we adopted the simplest model giving an adequate fit to the data and report the parameters derived from that description.

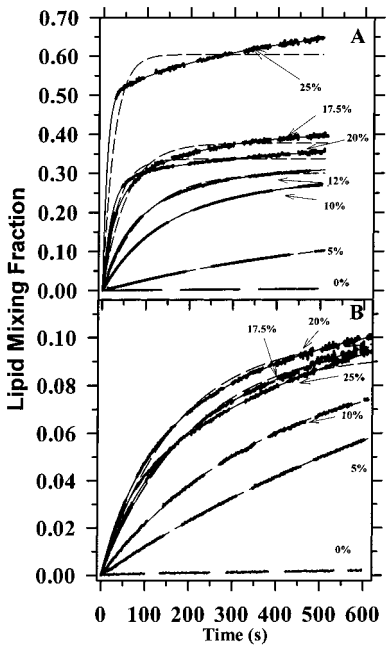


FIGURE 1: Time courses of lipid mixing fraction at different PEG concentrations. The mixing of lipids between PEG-aggregated DOPC:$DL_{18:3}$PC (85:15) (A) SUVs and (B) LUVs was measured using the Bodipy membrane mixing assay (see Methods). PEG concentrations of 0, 5, 10, 12, 17.5, 20, and 25 wt % were used, as indicated in the figure. A control experiment done at 0 wt % PEG showed no lipid mixing. Data are shown as bold dashed lines with noise, while the smooth thinner lines lines are fits of a single (dashed) or double (solid) exponential model to the data. The 5 and 10 wt % PEG data are shown fit to a single-exponential model (thin dashed lines), since the two fits were indistinguishable.

## RESULTS

*Outer Leaflet Mixing Precedes Inner Leaflet Mixing, but without a Lag Phase.* Fusion was first detected, without any significant leakage (<1%), in DOPC:$DL_{18:3}$PC 45 nm vesicles at 17.5 wt % PEG (*13*, *14*). Beyond 20 wt % PEG, these vesicles ruptured significantly (*13*). For the 20 nm vesicles examined here, we show in Figure 1A that there was significant lipid transfer between vesicles below these PEG concentrations. A finite rate of lipid mixing was observed even at 5 wt % PEG. As PEG concentration increased above 5 wt %, the rate of lipid mixing increased gradually. While the time course of lipid mixing was described reasonably well by a single exponential from 5 to 12 wt % PEG (see dashed lines in Figure 1A), time courses obtained above 12 wt % PEG concentration required two exponentials for an adequate description (see solid lines in Figure 1A), consistent with there being more than one lipid rearranging event occurring during the fusion process, as previously observed for 45 nm vesicles (*14*). The rate constants and extents of lipid mixing at infinite time are

Table 1: Time Constants and Preexponential Factors for Fusion Events at 23 °C[a]

| | parameters[b] | | | | |
|---|---|---|---|---|---|
| assay (wt % PEG) | $y_1$ (% total) | $y_1$ | $y_2$ | $\tau_1$ (s) | $\tau_2$ (s) |
| LM−SUVs (fraction) | | | | | |
| 5% | | 0.181 ± 0.001 | | 608 ± 3 | |
| 10% | | 0.277 ± 0.003 | | 149 ± 1 | |
| 12% | | 0.301 ± 0.004 | | 92 ± 1 | |
| 17.5% | 57 | 0.231 ± 0.002 | 0.174 ± 0.002 | 24 ± 0.4 | 171 ± 4 |
| 20% | 75 | 0.280 ± 0.001 | 0.092 ± 0.001 | 19 ± 0.2 | 302 ± 10 |
| 25% | 72 | 0.502 ± 0.001 | 0.192 ± 0.001 | 9 ± 0.1 | 362 ± 48 |
| LM−LUVs (fraction) | | | | | |
| 5% | | 0.129 ± 0.001 | | 1030 ± 5 | |
| 10% | | 0.092 ± 0.001 | | 372 ± 5 | |
| 17.5% | 36 | 0.050 ± 0.003 | 0.088 ± 0.006 | 114 ± 4 | 822 ± 67 |
| 20% | 40 | 0.047 ± 0.002 | 0.070 ± 0.001 | 83 ± 2 | 421 ± 20 |
| 25% | 27 | 0.034 ± 0.001 | 0.092 ± 0.001 | 59 ± 1 | 580 ± 16 |
| ILM (%) | | | | | |
| 17.5% | | | 0.109 ± 0.003 | | 267 ± 34 |
| 20% | | | 0.351 ± 0.004 | | 203± 9 |
| CM (%) | | | | | |
| 17.5%[c] | | | 0.095 ± 0.001 | | 351 ± 5 |
| 20% | 54 | 0.253 ± 0.014 | 0.217 ± 0.010 | 61 ± 2 | 274 ± 29 |
| contents leakage (fraction) | | | | | |
| 5% | | | 0.015 ± 0.005 | | >10000 |
| 10% | | | 0.019 ± 0.004 | | 309 ± 29 |
| 12% | | | 0.022 ± 0.003 | | 344 ± 16 |
| 17.5% | | | 0.036 ± 0.002 | | 347 ± 30 |
| 20% | 38 | 0.046 ± 0.001 | 0.075 ± 0.001 | 37 ± 1.2 | 256 ± 11 |
| 25% | 52 | 0.146 ± 0.002 | 0.137 ± 0.001 | 15 ± 0.3 | 199 ± 6 |
| TBM ratio | | | | | |
| 17.5% | | | 0.0164 ± 0.002 | | 217 ± 27 |
| 20% | 46 | | 0.0604 ± 0.004 | | 150 ± 27 |
| packing changes[d] ($\tau_{D_2O/H_2O}$) | | | 0.067 ± 0.001 | | 475 ± 2 |

[a] Abbreviations: LM, lipid mixing; ILM, inner leaflet mixing; CM, contents mixing; TBM, transbilayer movement. [b] Parameters from $y_1[1 - \exp(-k_1x)] + y_2[1 - \exp(-k_2x)]$. For trans-membrane ratio data, $y_1$ and $y_2$ are increases relative to an intercept value of $y_0$. [c] No contents mixing was detected at PEG concentrations of <17.5 wt % (see Figure 3). [d] Parameters from $y_o + y_1 \exp(-k_1x)$.

recorded in Table 1, which shows that the fast component dominated once fusion began. The rates of the fast and slow components for 17.5 wt % PEG ($t_{1/2} \approx 24$ and 171 s, respectively) were comparable to those we have reported for 45 nm vesicles (*14*). While both a rapid and a slow intervesicle lipid mixing were observed, there was no lag phase separating them, as we have previously seen in 45 nm vesicles ($t_{1/2} \approx 10$ and 150 s, respectively) (*14*). It is interesting to note that the "extent of lipid mixing" as monitored at a set time (300 s) remained nearly constant (27−36%) over the PEG concentration range of 10−20 wt %, as we have reported previously for several lipid compositions (*19*, *35*). We have pointed out that the extent of lipid mixing between aggregated vesicles is limited by the kinetics of aggregation (*36*), so it is not unreasonable that the extent of lipid mixing should be roughly independent of PEG concentration once aggregation occurs efficiently and rapidly.

To examine lipid rearrangements in membranes of larger size, we monitored lipid mixing between LUVs at the same PEG concentrations used with 20 nm SUVs (Figure 1B). Total lipid mixing increased with increased PEG as it did for SUVs, but the rate at any PEG concentration was at most half that seen for SUVs. The two-step process of lipid mixing in LUVS was never dominated by the fast component (Table 1) and the extent of lipid mixing was never greater than 13%. As for SUVs, there was no lag phase, so three distinct processes could not be detected. It seems also that 100 nm vesicles do exchange lipids between their outer leaflets when aggregated by 5 wt % PEG.

Previously our lab showed that lipid mixing was highly temperature dependent (*12*). This translated into activation energies for formation of the fusion intermediates that were comparable to those reported for analogous kinetic events recorded for viral and secretory vesicle fusion. To gain insight into the nature of the lipid rearrangements monitored by our lipid mixing assay, we monitored the time course of lipid mixing in highly curved SUVs at 5 (Figure 2 A), 10 (Figure 2B), and 17.5 (Figure 2C) wt % PEG at three different temperatures to determine the activation energy of outer leaflet mixing (only process occurring at 5 wt % PEG) and the activation energy of complete lipid mixing at fusion (17.5 wt % PEG). Lipid mixing was a slow, single-step process at 5 wt % PEG, whose rate increased with increased temperature (Figure 2A). However, lipid mixing at 10 and 17.5 wt % PEG was described by two exponentials. The fast component of 17.5 wt % PEG was more temperature dependent than the slow component (Figure 2C). We will analyze these data in terms of Arrhenius plots in the Discussion.

*Contents Mixing First Observed at 17.5 wt % PEG, but without Initial Lag Phase.* As documented in Figure 3, contents mixing was not detectable below 17.5 wt % PEG, as we have reported previously for 45 nm vesicles based on single time measurements (*13*). One exponential was required to describe the time course of contents mixing at 17.5 wt % PEG, while two exponentials were needed for 20 wt % (Table 1). Figure 3 also reports that leakage could be

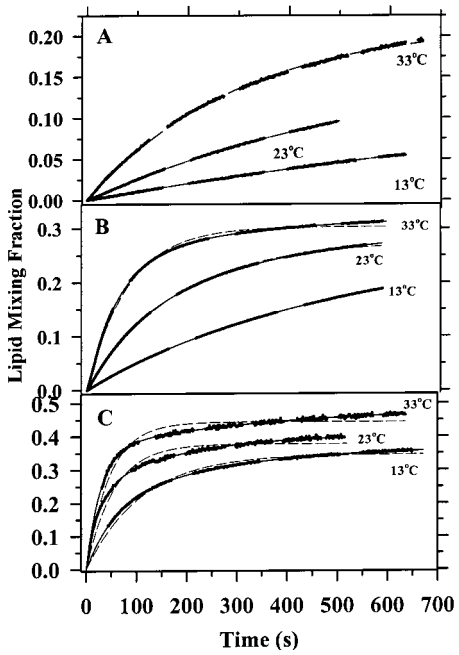


FIGURE 2: Time courses of the fraction of lipid mixing at three temperatures are shown for DOPC:$DL_{18:3}$PC (85:15) SUVs at (A) 5, (B) 10, and (C) 17.5 wt % PEG. Data are shown by thick dashed lines with noise, while fits are shown as thin solid (double exponential) or thin dashed (single exponential) lines.

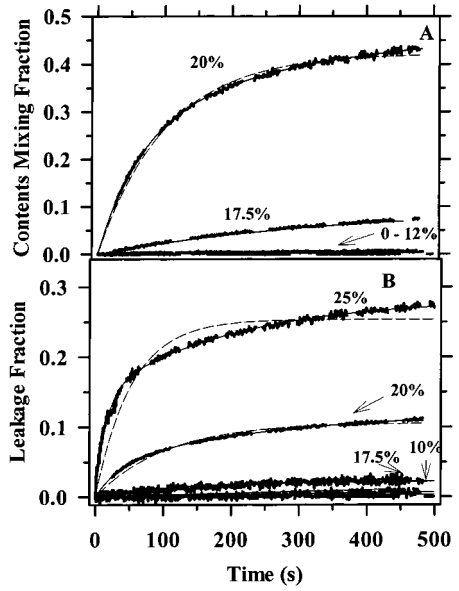


FIGURE 3: Time courses of the fraction of contents mixing as between DOPC:$DL_{18:3}$PC SUVs during PEG-mediated fusion. The change in fluorescence of $Tb^{3+}$ in complex with DPA (see Methods) was measured using PEG concentrations of 0, 5, 10, 12, 17.5, 20, and 25 wt %. The assay monitored a change in fluorescence due to (A) contents mixing, or (B) contents leakage of the $Tb^{3+}$/DPA complex. Data and fits are labeled as in Figure 2. A double exponential analysis of data at 17.5 wt % PEG is not presented since the regression did not converge.

described by a single exponential and was minimal but still detectable ($\sim 3.2 \times 10^{-3}$ %/s; Table 1) at 10 wt % (where no fusion was detected) and 17.5 wt % PEG ($2.8 \times 10^{-3}$/s, where fusion was first detected). The fact that leakage was observed at nearly identical rates just below and at the fusion threshold of PEG suggests that leakage and fusion are processes that are not directly related, at least at these low PEG concentrations, which is consistent with previous reports

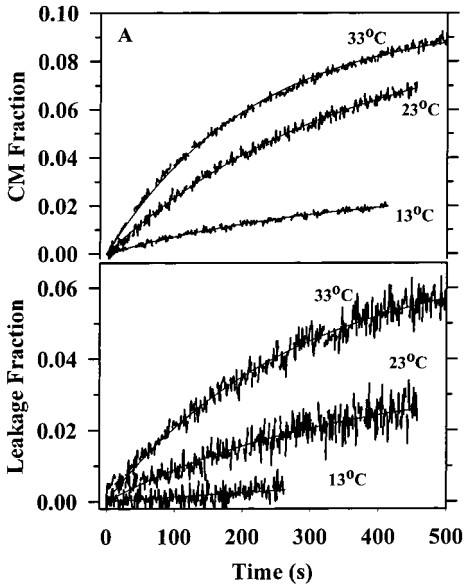


FIGURE 4: Time courses of the fraction of (A) contents mixing between and (B) contents leakage from DOPC:$DL_{18:3}$PC (85:15) SUVs at three temperatures (13, 23, and 33 °C). Data are labeled as in Figure 2, but single-exponential fits are shown as thin solid lines.

(*27*, *37*). Contents leakage required a two exponential description at 20 wt % PEG (Table 1). Above 25 wt % PEG, these vesicles exhibited a very rapid initial mixing of contents, followed by a decrease in contents mixing (data not shown) due to significant leakage.

To gain further insights about the fusion intermediates and compare with results found for lipid mixing at 17.5 wt % PEG, we monitored contents mixing at three temperatures (Figure 4) to determine the activation energy of pore formation. Contents mixing (Figure 4A) and leakage (Figure 4B) at 17.5 wt % PEG both remained single-step processes at all three temperatures examined.

*Inner Leaflet Mixing Occurs without Delay*. Inner-leaflet mixing should correlate with mixing of contents between fusing vesicles (*14*). To test for this, we monitored inner-leaflet lipid mixing at the PEG concentrations where we detected contents mixing without significant contents leakage. Inner-leaflet lipid mixing started almost immediately after addition of 17.5 wt % PEG (within 10 s) and was well described by a single exponential (Figure 5, Table 1). At 20 wt % PEG, it was also well described by a single-exponential rise as evidenced from the double-exponential fit shown by the solid line in Figure 5. In addition, the rate of the slow component of total lipid mixing at both 17.5 and 20 wt % PEG agreed reasonably well with the rate of inner leaflet mixing (Table 1). This suggests that the slow component of lipid mixing corresponds to inner leaflet mixing, as might be expected.

*Transbilayer Movement of Lipids (from Outer Leaflet to Inner) Occurs during the Fusion Process*. By following the exposure of NBD-PS to dithionite, as described in Methods, lipids were found to move from the outer to the inner leaflet of SUVs during fusion induced by 17.5 or 20 wt % PEG (Figure 6). The trans-bilayer movement of lipids was well described by a single-exponential model at 17.5 wt % PEG (dashed curve in Figure 6), but showed features of a two-exponential process at 20 wt % PEG (solid curve in Figure

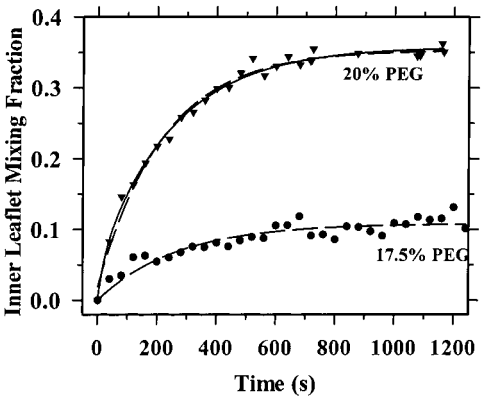


FIGURE 5: Fraction of inner leaflet mixing between DOPC:$DL_{18:3}$PC SUVs during PEG-mediated fusion. The mixing of inner leaflets of 0.5 mM SUVs was measured using NBD-PS (see Methods) at PEG concentrations of 17.5 and 20 wt %. The dashed lines result from fitting the data to a single-exponential function, the solid line through the 20% data is due to a double exponential.

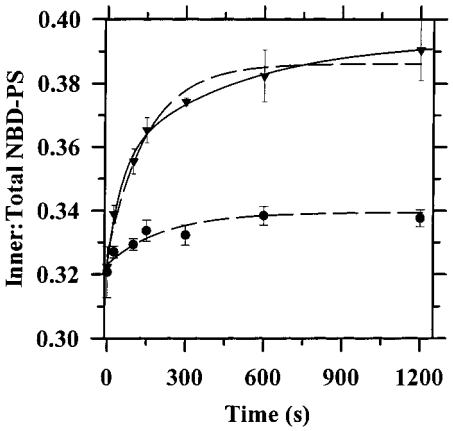


FIGURE 6: Time course of the change in ratio of inner-to-total leaflet probe as measured in DOPC:$DL_{18:3}$PC SUVs during PEG-mediated fusion. The trans-bilayer movement (TBM) of lipids was detected in SUVs during fusion at 17.5% (circle) and 20% PEG (inverted triangle) using NBD-PS as the fluorescence probe as described in the Methods. The dashed lines derive from single-exponential fits to the data, the solid line is due to a double-exponential fit of the 20% data.

6). However, when considered in the context of the error bars on these measurements, there was no compelling reason to assume the more complex double-exponential model and the parameters given in Table 1 are those for the single-exponential model (dashed curve). The rates seen at both 17.5 and 20 wt % PEG are quite similar both to rates of inner leaflet mixing and to the slow component of total lipid mixing.

*Water Was Excluded from the Bilayer during Fusion at 17.5 wt % PEG*. SUVs have highly curved bilayers that experience significant outer-leaflet negative curvature stress leading to water penetration into the interfacial region of the bilayer (*27*). Relief of this curvature stress could drive the fusion process. To determine when during the fusion process this negative curvature stress might be relieved, we added TMA-DPH to vesicles, fused them in buffer with 17.5 wt % PEG, and measured the fluorescence lifetime of TMA-DPH over time. To ascertain if TMA-DPH was exposed to water during the fusion process, this measurement was repeated in $D_2O$. These measurements were repeated in the absence of PEG as a control. The ratio $\tau_{ave}^{D_2O}/\tau_{ave}^{H_2O}$, which has been

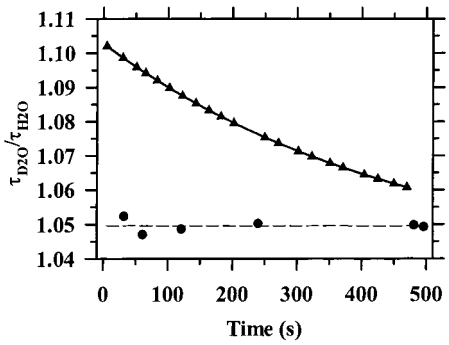


FIGURE 7: Time variation of the ratio of TMA-DPH lifetimes in $D_2O$ and $H_2O$ ($\tau_{D_2O/H_2O}$) during PEG-mediate fusion at 0 (circle) and 17.5 (triangle) wt % PEG. TMA-DPH was added to vesicles prior to addition of PEG to initiate fusion and allowed to incubate 10 min before measurements (see Methods). The solid lines derive from single-exponential fits to the data.

proposed to be a measure of water penetration into the interface region of the bilayer (*32*), showed a gradual decrease during fusion (Figure 7), whereas there was no change in the ratio when there was no PEG present. Since a $\tau_{ave}^{D_2O}/\tau_{ave}^{H_2O}$ ratio of 1 indicates that exchangeable protons are in a water-free environment, this result indicates that water was slowly excluded from the interface region of the bilayer during the fusion process. Since this occurred with a time constant slower than the slowest lipid rearrangement observed, there are several possible explanations of this behavior.

## DISCUSSION

*Lipid Mixing Reflects Formation of the Initial Hemi-Fused Intermediate at 5 and 10 wt % PEG but Probably Several Unresolved Steps at Fusing PEG Concentrations.* The kinetic constants for processes associated with PEG-mediated SUV fusion are summarized in Figure 8. These provide a fairly detailed picture of the lipidic rearrangements that are associated with fusion between 20 nm vesicles that are held in contact by PEG. PEG-mediated fusion begins with the outer leaflets of SUVs coming into contact with one another and intermixing. In the presence of 5−12 wt % PEG, lipid mixing (circles in Figure 8), presumably mainly between contacting outer leaflets, is the main process that occurs, as indicated by the lack of contents mixing (triangles) at these PEG concentrations (Figure 3) and by a decent description of lipid mixing in terms of a single exponential. At 5 wt % PEG, where inter-bilayer separation is greatest, only a very slow process ($\tau \approx 608$ s; Table 1) is seen. This implies either that inter-vesicular contact is not continuous at 5 wt % PEG and lipid mixing is facilitated by fluctuations that bring bilayers into contact with a small probability that increases with decreasing inter-bilayer distance (*11*) or that vesicles come close to one another without contacting, such that there is inter-vesicular lipid exchange through a thin inter-bilayer layer of altered aqueous medium (*36*). The latter explanation would predict a continuous decrease of activation energies with increasing PEG concentration, leading to increased rates, while the former could accommodate a roughly invariant activation energy at increasing PEG concentrations. Our observation of roughly the same activation energy at 5 and 10 wt % PEG (Figure 9B; Table 2) favors the former explanation. The smooth variation of the fast component of

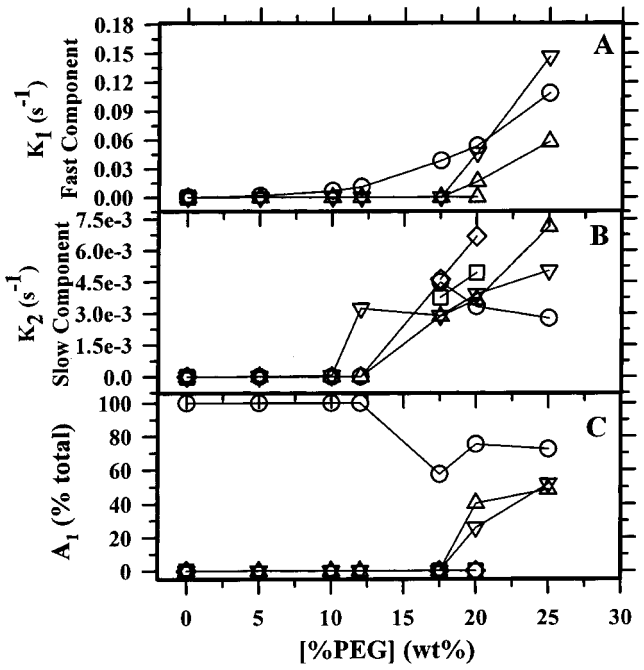


FIGURE 8: Variation of the kinetic parameters for events occurring during fusion induced by different PEG concentrations. Plotted are the fast components (A), the slower components (B), and the preexponential factor of the fast component (as a percent total) (C) for lipid mixing (LM, circles), inner leaflet mixing (ILM, squares), contents mixing (CM, triangles), trans-bilayer movement (TBM, diamonds), and contents leakage (inverted triangles) in DOPC:$DL_{18:3}$PC (85:15) SUVs.

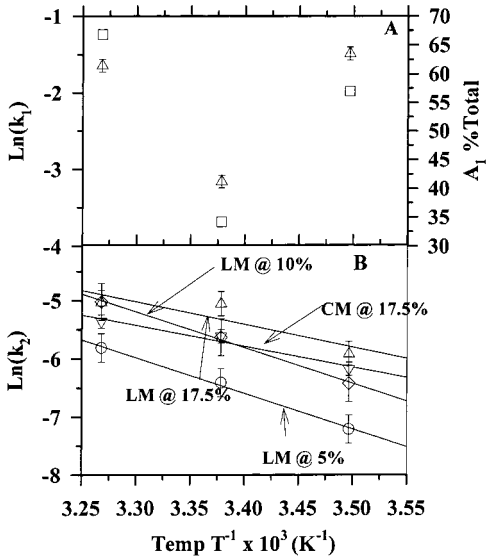


FIGURE 9: Arrhenius plots of the exponential constants associated with (A) the fast component of lipid mixing at 17.5 wt % PEG (triangles) and (B) the slow component of lipid mixing at 5 (circles), 10 (diamonds), and 17.5 (triangles) wt % PEG, and contents mixing (inverted triangle) at 17. 5 wt % PEG. The percent of total change associated with the fast component of lipid mixing is also shown in frame A (squares). Error bars on each point derive from the uncertainties in fitting parameters of experimental time courses.

lipid mixing with PEG concentration (circles in Figure 8A) suggests that the merging of outer leaflets seen below the fusion threshold is related to the formation of the initial intermediate. However, the activation energy of this process (12−15 kcal/mol obtained at 5 and 10 wt % PEG) is less than half that previously reported for formation of the initial intermediate

Table 2: Arrhenius Activation Energies for Fast ($E_1^{\pm}$) and Slow ($E_2^{\pm}$) Processes Associated with Fusion[a]

| % PEG | lipid mixing | | contents mixing $E_{a2}$ |
|---|---|---|---|
| | $E_{a1}$ | $E_{a2}$ | |
| 5% | 12.2 ± 0.8 | NO | NO |
| 10% | 15.5 ± 0.9 | NA | NO |
| 17.5% | non-Arrhenius behavior | 8 ± 4 | 7.1 ± 1.4 |

[a] NO, not observed. NA, the 10 wt % PEG data were adequately described by a single exponential except at 33 °C. Thus, we could not apply physical meaning to the two-exponential behavior of these data at 33 °C. So, we estimated the rate constant at 33 °C either using the single-exponential fit or using the calculated initial rate constant ($f_1k_1 + f_2k_2$, where $f_1$ and $f_2$ are the fractions of the total lipid mixing resulting from the fast and slow components, respectively). The same Arrhenius plot resulted in either case.

in 45 nM vesicles [37 kcal/mol (*12*)]. This could mean either that lipid mixing below the fusion threshold is not related to formation of the initial fusion intermediate or that the activation energies of formation of the initial intermediate are different in 45 and 20 nm vesicles. Although our data cannot rigorously distinguish between these two possibilities, we favor the later explanation for two reasons.

First, the single-exponential description of lipid mixing time courses was not perfect as we approached the threshold of fusion (i.e., at 12 wt % in Figure 1A). Once the fusion threshold was reached (17.5 wt % PEG), lipid mixing became distinctly biexponential, but it had a slight double-exponential character even at 12 wt % (compare dashed and solid lines in Figure 1A). This could reflect either a small amount of trans-bilayer movement or the existence of two types of lipid movements between vesicles. Since lipid trans-bilayer movement from the outer to inner leaflet does not occur below the fusion threshold (*38*), this implies two types of inter-vesicle lipid movement, with the nature of the lipid mixing process varying in a continuous fashion as one approaches and then passes the fusion threshold. Thus, a transient structure involving some joining of inner leaflets [like the transient pore reported for 45 nm vesicles (*14*)] could precede pore formation. Alternatively, both types of hemi-fusion intermediate, the stalk and the septum (*14*), could occur, with the probability of the second intermediate increasing as bilayers are driven into closer contact by PEG. Whatever be the case, our result implies that lipid rearrangements characteristic of fusion do not occur discontinuously at 17.5 wt % but that the lipid rearrangements leading to fusion simply become increasingly probable as bilayers are brought closer together. If so, we would expect that the lipid mixing process does not change in its basic nature between 5 and 17.5 wt %, but changes only in the particular admixture of component processes that contribute at different inter-bilayer separations. Thus, we would expect the activation energies of lipid mixing at 5 and 10 wt % PEG to be comparable (as seen) and similar to that of the formation of initial intermediate at 17.5 wt %, which we could not obtain. The fact that the fast component of lipid mixing does not follow a simple Arrhenius model at 17.5 wt % PEG (Figure 9A) is consistent with one of these processes becoming more dominant, but in a highly temperature-dependent fashion, at the fusion threshold.

Second, the activation energies derived from the Arrhenius plots for the slow component of lipid mixing (Figure 9B,

triangles; 8 kcal/mol) and for the mixing of contents (Figure 9B, inverted triangles; 7.1 kcal/mol) were in good agreement, consistent with the interpretation that the slow component of lipid mixing that appears at 17.5 wt % PEG (Table 1) corresponds to inner leaflet mixing associated with pore formation. The values obtained for this process are also roughly a third of the values obtained for 45 nm vesicles [21−22 kcal/mol (*12*)], suggesting that the high curvature of SUVs lowers the barrier to pore formation. Thus, it is reasonable to expect that high curvature lowers the barrier to formation of the initial intermediate, which is what we see if the activation energy of lipid mixing at 5 and 10 wt % PEG in 20 nm vesicles (12−15 kcal/mol) is compared to that seen in 45 nm vesicles at the fusion threshold [37 kcal/mol (*12*)].

*High Curvature Affects both Steps in the Fusion Process*. What is remarkable about our lipid mixing data for SUVs is that the rate of initial intermediate formation in 20 nm vesicles (1/24 $s^{-1}$, Table 1) was comparable to the rate we observed for 45 nm vesicles [1/11 $s^{-1}$ (*14*)]. We have reported a similar surprising result elsewhere (*39*). As mentioned above, we adopt the view that formation of the initial intermediate is proportional to the probability of close contact between closely apposed fluctuating bilayers times the exponential of the activation energy for formation for the first intermediate (*11*). In this view, the fact that the activation energy for outer-leaflet lipid mixing is a bit less than half of the value estimated for the formation of the first intermediate in 45 nm vesicles means that the probability of points of inter-bilayer contact that can develop into initial fusion intermediates must be greater for 45 nm than for 20 nm vesicles. This is as expected for comparison of two vesicles with different surface curvature and rigidity (*39*). Thus, the comparable rates seen for lipid mixing in fusing 20 and 45 nm vesicles seems to reflect compensating effects of curvature.

Curvature seems also to affect the later stages of the fusion process. First, as mentioned above, the activation energy for pore formation was clearly lowered by the increased curvature of 20 nm vesicles. Second, although fusion did not occur at all under our PEG concentrations (0−25 wt % PEG) in LUVs [Table 1 and (*35*)], lipid mixing between LUVs still required two exponentials for an adequate description at 17.5 wt % PEG and above (Figure 1B and Table 1). This implies that two types of lipid-mixing intermediates form in this PEG concentration range in essentially uncurved LUVs but that these cannot evolve to a fusion pore. This is consistent with an increase in activation energy for this step with the decreasing curvature of LUVs, as discussed above when comparing 20 and 45 nm vesicles.

*Fusion of SUVs Is a Three-Step Process*. Although inner leaflet mixing, contents mixing/leakage, and trans-bilayer movement do not all occur until 17.5 wt % PEG, these events all appear to occur almost simultaneously, with outer leaflet mixing not being distinguishable as an initial step in the early stages of fusion (Figures 1, 3, 5, 6). This potentially conflicts with our observation of three distinguishable events during PEG-mediated fusion of 45 nm vesicles (*14*). This means either that fusion follows a fundamentally different course in SUVs as opposed to the intermediate sized vesicles we have previously characterized or that the free energy of either the first or second intermediate is altered so that the three steps of the process cannot be resolved in SUVs. Our data suggest the latter. The failure of the Arrhenius plot for the rate of the fast component of lipid mixing to fit to a straight line (Figure 9A) is clearly consistent with this rate constant describing more than one kinetic event, with the contributions of the component events varying with temperature. We showed above that the slow component of lipid mixing in SUVs corresponds to inner leaflet mixing and pore formation from the second, committed intermediate (Table 1). This implies that the second kinetic process associated with the fast component of lipid mixing in 20 nm vesicles is conversion of the initial transient intermediate to the second, committed intermediate (*14*). It seems that the initial intermediate is so unstable in highly curved SUVs that it converts rapidly, especially at high temperature, to the second, committed intermediate, which then must decay to a pore. In SUVs of other compositions, we have also failed to observe three clearly defined steps in the fusion process. Only for vesicles prepared by incomplete sonication, detergent treatment, and dialysis from DOPC/phosphatidylethanolamine/sphingomyelin/cholesterol/phosphatidylserine have we observed a three-step process (Haque, Dennisen, Lentz, unpublished results). The free energy diagram for fusion seems to depend on vesicle geometry and composition in complex ways that only a detailed theoretical analysis can hope to predict.

*Lipids Move from Outer To Inner Leaflets at A Rate Similar to That of Inner Leaflet Mixing and Contents Mixing*. We have shown previously that lipids redistribute from the outer to the inner leaflet as 45 nm vesicles are induced to fuse by PEG (*13*). This is not to be confused with what we call "flip-flop", or scrambling of lipids between two leaflets. This process has been shown not to occur in either biological membrane (*40*) or PEG-mediated model membrane (*13*) fusion. Instead, we have measured a directed net movement of lipids toward the inner leaflets of vesicles during fusion. The necessity of this directed movement of lipids during SUV fusion has been noted previously (*13*), although its timing during the fusion process has not been known. Lipid trans-bilayer movement showed time courses quite similar to those of contents mixing and inner leaflet mixing at 17.5 and 20 wt % PEG (Table 1). This would suggest that trans-bilayer movement occurs with the initial formation of the fusion pore and may continue with the spreading of the fusion pore. The clustering of rates of contents mixing (triangles), inner leaflet mixing (squares), slow lipid mixing (circles), and trans-bilayer movement (diamonds) in Figure 8B implies that all these events are involved in pore formation and maturation. We note that leakage also occurs at a comparably slow rate under these conditions. We have noted previously that trans-bilayer lipid "flip-flop" could result from leakage and had carefully controlled for leakage so as to avoid such lipid scrambling (*13*). The question also arises as to whether leakage and pore formation might be related. We note elsewhere that the two processes often occur under similar conditions but that observation of clear contents mixing in the absence of any detectable leakage means that they are not intrinsically related (*13*, *37*).

*Water Is Excluded from the Bilayer Outer Leaflet after Pore Formation but This Seems Not to Drive Fusion*. Outer leaflet packing stress leading to water penetration has been argued to be necessary and perhaps sufficient for PEG-

mediated vesicle fusion (*13*, *17*, *19*, *27*, *35*). This implies that relief of outer-leaflet packing stress might contribute to driving fusion. We examined this possibility using the water-sensitive probe TMA-DPH. The variation of TMA-DPH lifetime ratio $\tau_{avg}^{D_2O/H_2O}$ during the fusion of SUVs shows that water is excluded from the bilayer during the fusion process at 17.5 wt % PEG (Figure 7). More interesting is the slow time scale over which this occurs (exponential decay constant $\approx$ 475s). This is considerably slower that any of the other detectable events of fusion. Since this time scale is longer than that of contents mixing ($\tau \approx$ 351s), this suggests that packing stresses are not relieved until after the fusion pore has formed and possibly started to mature. There are several possible explanations for this behavior. First, it could reflect slow annealing of the bilayer structure of the fusion product that is necessary for full exclusion of water from the outer leaflet of the fusion product. Second, it could reflect a gradual increase in the area of contact between vesicles as fusion proceeds to larger, more flexible vesicles. Finally, SUVs experience osmotic stress under the influence of PEG unless special efforts are made to match inner and outer osmolality (*39*). A compressive osmotic stress would be expected to force water into the interface region of the SUV outer leaflet. Although leakage was minimal under the conditions of our experiments (Figure 3 and Table 1), even a small amount of leakage could help relieve this osmotic stress and thus exclude water from the bilayer. Whatever be the explanation, the very slow time course of the change in $\tau_{ave}^{D_2O}/\tau_{ave}^{H_2O}$ makes it unlikely that relief of packing stresses are a significant driving force for fusion. If they were, we would have expected to find $\tau_{ave}^{D_2O}/\tau_{ave}^{H_2O}$ decreasing at the same rate at which fusion occurred. Since we did not, we conclude that, while outer leaflet packing stresses might help lower the barrier to forming the initial intermediate, these stresses are not relieved until late in the fusion process and their relief is probably unimportant in driving fusion.

## ACKNOWLEDGMENT

We would like to thank Dr. S. Moses Dennison for assistance with measuring the kinetics of lipid mixing at 10 wt % PEG.

## REFERENCES

1. Razinkov, V. I., Melikyan, G. B., and Cohen, F. S. (1999) *Biophys. J. 77* (6), 3144−51.
2. Kelsey, D. R., Flanagan, T. D., Young, J., and Yeagle, P. L. (1990) *J. Biol. Chem. 265* (21), 12178−83.
3. Ghosh, J. K., Peisajovich, S. G., and Shai, Y. (2000) *Biochemistry 39* (38), 11581−92.
4. Alvarez de Toledo, G., Fernandez-Chacon, R., and Fernandez, J. M. (1993) *Nature 363* (6429), 554−8.
5. Amatore, C., Bouret, Y., and Midrier, L. (1999) *Chem.—Eur. J. 5* (7), 2151−62.
6. Monck, J. R., and Fernandez, J. M. (1992) *J. Cell Biol. 119* (6), 1395−404.
7. Rauch, C., and Farge, E. (2000) *Biophys J. 78* (6), 3036−47.
8. Lentz, B. R., Malinin, V., Haque, M. E., and Evans, K. (2000) *Curr. Opin. Struct. Biol. 10* (5), 607−15.
9. Brunger, A. T. (2001) *Curr. Opin. Struct. Biol. 11* (2), 163−73.
10. Lentz, B. R., and Lee, J. K. (1999) *Mol. Membr. Biol. 16* (4), 279−96.
11. Burgess, S. W., McIntosh, T. J., and Lentz, B. R. (1992) *Biochemistry 31* (10), 2653−61.
12. Lee, J., and Lentz, B. R. (1998) *Proc. Natl. Acad. Sci. U.S.A. 95* (16), 9274−9.
13. Lentz, B. R., Talbot, W., Lee, J., and Zheng, L. X. (1997) *Biochemistry 36* (8), 2076−83.
14. Lee, J., and Lentz, B. R. (1997) *Biochemistry 36* (21), 6251−9.
15. Bramhall, J. (1986) *Biochemistry 25*(11), 3479−86.
16. Schuh, J. R., Banerjee, U., Muller, L., and Chan, S. I. (1982) *Biochim. Biophys. Acta 687* (2), 219−25.
17. Lee, J., and Lentz, B. R. (1997) *Biochemistry 36* (2), 421−31.
18. Chen, P. S., Jr., Toribara, T. Y., and Warner, H. (1956) *Anal. Chem. 28*, 1756−8.
19. Lentz, B. R., McIntyre, G. F., Parks, D. J., Yates, J. C., and Massenburg, D. (1992) *Biochemistry 31* (10), 2643−53.
20. Lentz, B. R., Carpenter, T. J., and Alford, D. R. (1987) *Biochemistry 26* (17), 5389−97.
21. Mayer, L. D., Hope, M. J., and Cullis, P. R. (1986) *Biochim. Biophys. Acta 858* (1), 161−8.
22. Malinin, V. S., Hoque, M. E., and Lentz, B. R. (2001) *Biochemistry* (in press).
23. Meers, P., Ali, S., Erukulla, R., and Janoff, A. S. (2000) *Biochim. Biophys. Acta 1467* (1), 227−43.
24. McIntyre, J. C., and Sleight, R. G. (1991) *Biochemistry 30* (51), 11819−27.
25. Burgess, S. W., and Lentz, B. R. (1993) *Methods Enzymol. 220*, 42−50.
26. Wilschut, J., Duzgunes, N., Fraley, R., and Papahadjopoulos, D. (1980) *Biochemistry 19* (26), 6011−21.
27. Talbot, W. A., Zheng, L. X., and Lentz, B. R. (1997) *Biochemistry 36* (19), 5827−36.
28. Viguera, A. R., Mencia, M., and Goni, F. M. (1993) *Biochemistry 32* (14), 3708−13.
29. Weber, T., Zemelman, B. V., McNew, J. A., Westermann, B., Gmachl, M., Parlati, F., Sollner, T. H., and Rothman, J. E. (1998) *Cell 92* (6), 759−72.
30. Stryer, L. (1966) *J. Am. Chem. Soc. 88*, 5708−12.
31. Stubbs, C. D., Ho, C., and Slater, S. J. (1995) *J. Fluoresc. 5* (1), 19−28.
32. Ho, C., Slater, S. J., and Stubbs, C. D. (1995) *Biochemistry 34* (18), 6188−95.
33. Chattopadhyay, A., and London, E. (1987) *Biochemistry 26* (1), 39−45.
34. Huang, Z. J., and Haugland, R. P. (1991) *Biochem. Biophys. Res. Commun. 181* (1), 166−71.
35. Burgess, S. W., Massenburg, D., Yates, J., and Lentz, B. R. (1991) *Biochemistry 30* (17), 4193−200.
36. Wu, J. R., and Lentz, B. R. (1991) *Biochemistry 30* (27), 6780−7.
37. Massenburg, D., and Lentz, B. R. (1993) *Biochemistry 32* (35), 9172−80.
38. Lentz, B. R., Madden, S., and Alford, D. R. (1982) *Biochemistry 21*, 6799−807.
39. Malinin, V. S., Frederik, P., and Lentz, B. R. (2001) *Biophys. J.* (Submitted for publication).
40. Klotz, K. H., Bartoldus, I., and Stegmann, T. (1996) *J. Biol. Chem. 271* (5), 2383−6.

BI011508X